ACS central science

http://pubs.acs.org/journal/acscii

Research Article

Rapid On-Cell Selection of High-Performance Human Antibodies

David N. Philpott, Surath Gomis, Hansen Wang, Randy Atwal, Abdellali Kelil, Tanja Sack, Brandon Morningstar, Chris Burnie, Edward H. Sargent, Stephane Angers, Sachdev Sidhu, and Shana O. Kelley*

Cite This: *ACS Cent. Sci.* 2022, 8, 102−109

Read Online

ACCESS | Metrics & More | Article Recommendations | Supporting Information

ABSTRACT: Phage display is a critical tool for developing antibodies. However, existing approaches require many time-consuming rounds of biopanning and screening of potential candidates due to a high rate of failure during validation. Herein, we present a rapid on-cell phage display platform which recapitulates the complex *in vivo* binding environment to produce high-performance human antibodies in a short amount of time. Selection is performed in a highly stringent heterogeneous mixture of cells to quickly remove nonspecific binders. A microfluidic platform then separates antigen-presenting cells with high throughput and specificity. An unsupervised machine learning algorithm analyzes sequences of phage from all pools to identify the structural trends that contribute to affinity and proposes ideal candidates for validation. In a proof-of-concept screen against human Frizzled-7, a key ligand in the Wnt signaling pathway, antibodies with picomolar affinity were discovered in two rounds of selection that outperformed current gold-standard reagents. This approach, termed μCellect, is low cost, high throughput, and compatible with a wide variety of cell types, enabling widespread adoption for antibody development.

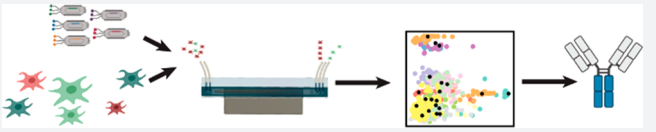

INTRODUCTION

Phage display is an antibody discovery tool that screens bacteriophage presenting a library of variable antibody domains against a target antigen. Through multiple rounds of incubation with the target, washing away unbound phage, and amplifying bound phage, the library is reduced to those clones with affinity and specificity to the antigen.[1,2] Individual clones can be selected or screened from this sublibrary and converted into an IgG format for use as diagnostic or therapeutic reagents.

Though effective, traditional phage display suffers from key limitations. Conventionally, >5 rounds of selection are required to generate clones with high affinity to the target. The cost and time requirements of repeat rounds (approximately 6−8 weeks and $8,000−10,000 USD in total) are a bottleneck in the discovery of new therapeutics.[3,4] The difficulty in controlling stringency during binding causes many candidates from the enriched phage pools to represent false positives that fail *in vitro* validation.[5,6] An inability to recapitulate the low relative concentration and morphology of targets *in vitro* may also lead to candidates failing later during *in vivo* testing.[7] The stochastic nature of selection results in thousands of nonspecific clones, requiring further screening for elimination. Further, variations in the efficiency of bacterial amplification result in candidates being missed due to low representation.[8,9]

To address these issues, variations of the phage display approach have been developed. These include performing selection with antigens presented on a cell surface[10] and with mixed cell types,[11] incorporating microfluidics to control the binding dynamics,[12,13] and using next-generation sequencing (NGS) and bioinformatics analysis to choose clones for validation, to further library design,[14] or to eliminate nonspecific clones.[15]

Although the feasibility of these approaches has been explored, a comprehensive platform combining these novel features to produce high-performing antibodies in a reduced number of rounds against a challenging therapeutic target has yet to be demonstrated.

In this paper, we present such a platform: μCellect. To recapitulate the *in vivo* binding environment, antigens are presented on the surface of a cell with a large background of nonspecific cell types. By modifying the ratio of cell types, different levels of stringency can be applied to the selection. To eliminate amplification bias, a very high sampling rate is achieved by using a large number of cells (>10^7). To choose clones, all phage pools are sequenced and an unsupervised machine learning algorithm selects top clones based on structural trends in the entire data set and enrichment scores. With this workflow, the number of rounds required to discover quality candidates is reduced. By using low-cost microfluidic devices and open-source software, the cost per round of

Received: September 30, 2021
Published: December 29, 2021

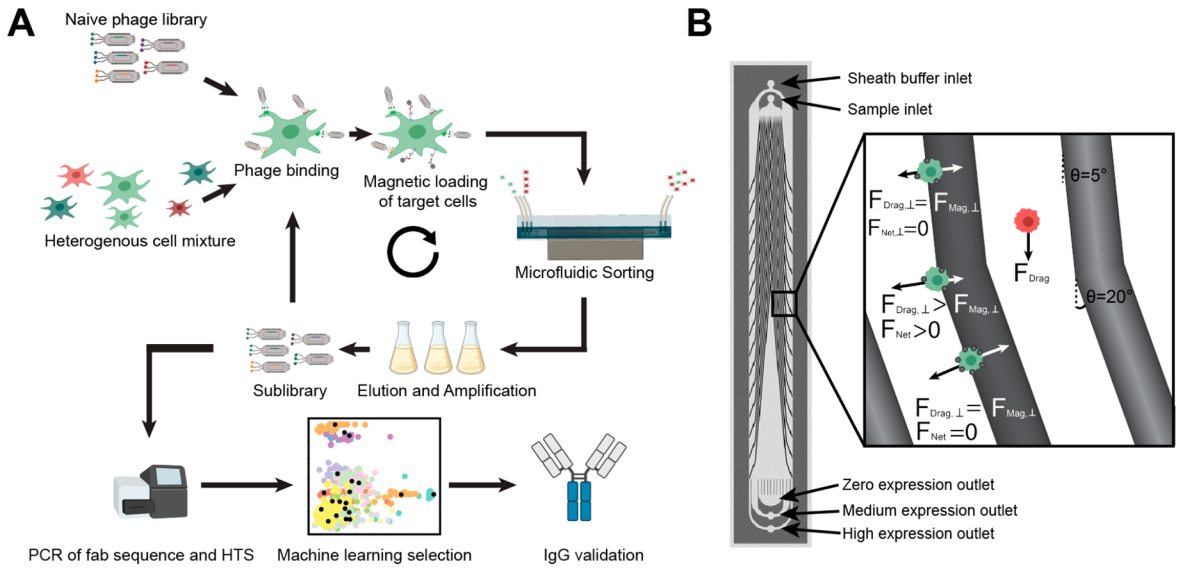

Figure 1. Overview of μCellect. (A) Schematic overview of the μCellect methodology. HTS: high-throughput sequencing. (B) The microfluidic cell sorter (MICS) chip uses patterned guides to separate cells based on protein expression. Deflection caused by combined Stokes' drag force (from fluid flow, toward outlets) and magnetic force (from labeling, toward the guides) acting on cells.

selection is also kept low, making it appealing for widespread deployment.

DESIGN OVERVIEW

μCellect (Figure 1A) begins with the incubation of a naïve phage library with a heterogeneous mixture consisting of a minority of cells expressing the target antigen and a large background of a cell type lacking the target. Target cells are then labeled with magnetic nanoparticles (MNPs) specific to a capture probe and sorted using a microfluidic cell sorter (MICS).[16]

The MICS device (Figure 1B) is a low-cost (<$50/chip), high-throughput (>10^7 cells/h) cell sorter. Target cells are deflected laterally by sets of angled guides which balance the Stokes' drag force (from fluid flow) and the magnetic force (from labeling). Phages are eluted from these selected cells and amplified to produce a phage sublibrary. The process is repeated for iterative enrichment, and all sublibraries are sent for next-generation sequencing (NGS).

The data produced is processed by an algorithm which first identifies sequences representing structural trends in the data set found by *k*-means clustering and then compares them to enrichment scores. Candidates that best represent the features contributing to antigen binding are selected for validation. The candidates are expressed in IgG format and validated. In a proof-of-concept screen, antibodies against human Frizzled-7 (Fzd7) with subnanomolar dissociation constants (K_d) were found in only two rounds of selection.

RESULTS

Testing of Microfluidic Cell Sorting (MICS) Platform for Antibody Selection. Polyclonal CHO cell lines recombinantly coexpressing human Fzd7 and GPI-anchored myc peptide tag, or myc tag alone, were created. Overexpression of human Fzd7 was required to overcome the background of hamster Frizzled orthologues. To capture as many of the target-expressing cells as possible and to have a tag independent of host cell function, exogenous myc tag with a GFP internal readout was used. CCK8 assays were used to optimize the antibiotic concentrations required to maintain a high expression of these constructs (Figure S1A,B). Labeling conditions were optimized to achieve a maximal magnetic loading of Fzd7$^+$myc$^+$ cells while maintaining specificity (Figure S1C). The cells were then sorted on the MICS device, and the flow rate was optimized to balance capture efficiency and throughput (Figure S1D).

At a nominal flow rate of 10 mL/h, over 90% of myc+ cells were captured with no capture of wild-type CHO cells. Phage binding was shown to have a minimal effect on cell capture (Figure 2A). To test the ratio of positive to negative cells that could be resolved on the MICS device, target cells were spiked into non-antigen-expressing cells and the sample was labeled and sorted (Figure 2B). A ratio of 1:200 target:nontarget cells were accurately recovered; a ratio of 1:20 was used for the antibody election screen.

Lastly, the performance of the MICS platform was benchmarked against other sorting technologies using metrics relevant to the phage display application (Figure 2C). Magnetic-activated cell sorting (MACS) had comparable throughput to MICS, but bound phages were lost during the sorting process, likely due to the aggressive flushing of target cells from the binding column. Fluorescence-activated cell sorting (FACS) had comparable phage recovery, but the slow processing speed presented a major limitation for processing large cell populations.

Biopanning. The phage library screening workflow consisted of two rounds of selection using Fzd7$^+$myc$^+$ target cells, and one subsequent counter selection with myc$^+$ cells as targets to identify clones binding to myc (Figure S1E). Library F, a synthetic human fab (fragment antigen binding) library containing 10^{13} uniquely mutated sequences in four (L3, H1, H2, and H3) of six complementarity determining regions (CDRs), was used for selection. CDR sequences are found at the very end of the variable region of an antibody and are the key determinants of epitope recognition.[17] For each round, 2×10^6 Fzd7$^+$myc$^+$ cells were mixed with 4×10^7 CHO cells transfected with similar plasmids that did not contain Fzd7 or myc. Using the optimized flow rate and running two MICS

https://doi.org/10.1021/acscentsci.1c01205
ACS Cent. Sci. 2022, 8, 102−109

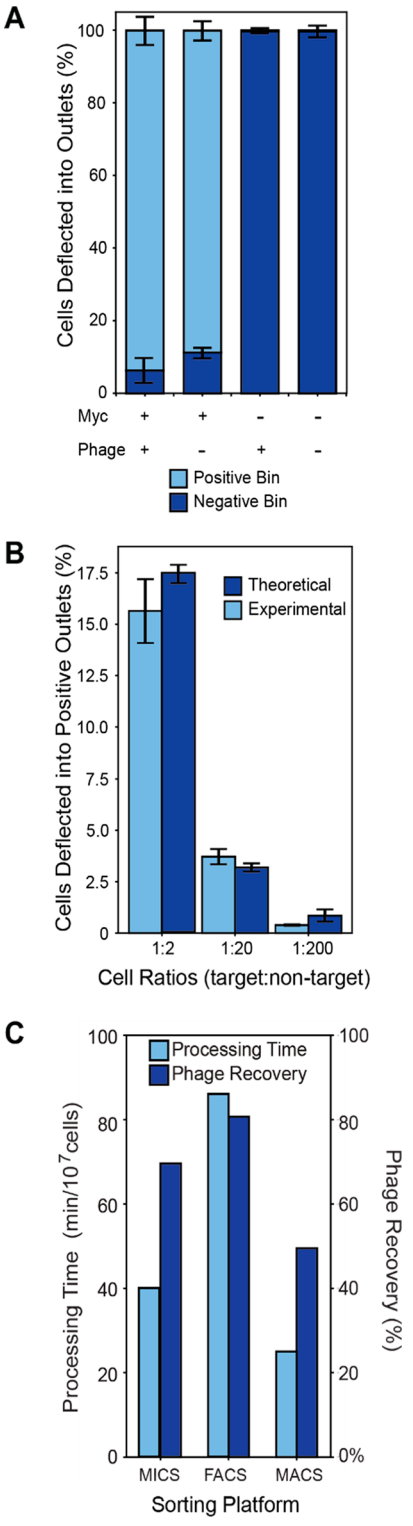

Figure 2. Optimization of microfluidic sorting. (A) Assessment of phage binding on sorting performance. Pure polyclonal cell lines with and without myc overexpression were used. Cells from the medium and high outlets were considered positive. Error bars indicate standard deviation across $N = 3$ technical replicates. (B) Recovery of spiked-in cell mixtures at various ratios compared to theoretical amounts. A ratio of 1:20 target:nontarget was used for the screen. Error bars indicate the standard deviation across $N = 3$ technical replicates. (C) MICS performance relative to other cytometry platforms, assessed by processing time and phage recovery.

chips in parallel, a throughput of 6×10^7 cells/h was achieved. Enriched outlet populations showed an 8-fold increase in GFP expression—the internal readout for myc expression. This data suggests that the sorting was highly selective (Figure S1F). After completion of the rounds, gDNA from all phage pools was extracted; the CDR-containing region was amplified by barcoded PCR, and samples were pooled and deep sequenced.

Data Analysis and Candidate Selection. Data from NGS underwent quality control and preliminary processing to remove poor-quality reads and identify mutated CDR regions.[7] Positive read counts were calculated by combining reads from the medium and high outlets of the MICS device. Reads from the unbound pool (phage collected from supernatant after cell incubation and before sorting) and the zero outlet were combined to generate a negative read count. A clonal enrichment score for each clone in each round was calculated by taking the −log2 ratio of negative to positive counts.[18] In round 1, the data set was dominated by low read count clones (Figure S2A) of which fewer than 1% were seen in later rounds. Therefore, we concluded that they were likely noise. Round 2 was more normally distributed (Figure S2B) thus we exclusively used this data set for enrichment analysis. Clones enriched in the myc counter selection (907 clones) were also removed leaving 24 350 unique clones in round 2.

We opted to develop an unsupervised *k*-means approach to candidate selection (Figure 3A). This approach first clustered all sequences in the data set by shared homology, and a centroid sequence was generated which best represents the shared motifs in that cluster. The number of clusters which sequences were binned into, the *k*-value, was not optimizable by the elbow method due to high variance, so many *k*-values and runs were compared (20, 150, 300, and 500). Next, a cluster enrichment score was calculated by dividing the mean clone enrichment score by the standard deviation of clones within the cluster. We hypothesized that clusters with a high cluster enrichment score would contain centroid sequences which had the most promise of successful validation. Additionally, we hypothesized that the larger the cluster size, the stronger the trend was in the data, and we could have a greater degree of confidence that the centroid sequence would validate.

To develop this approach, we first analyzed whether clustering by concatenated CDR sequences or by individual CDRs contributed most toward cluster enrichment scores. *k*-means clustering with $k = 20$, using either the concatenated sequence or individual CDRs, was performed and compared to the cluster enrichment score (Figure 3B). Clustering by $k = 20$ was chosen to ensure that the same *k*-value could be used for all permutations, since clustering by individual CDRs did not have enough diversity to support higher *k*-values. This analysis revealed that concatenated sequences had the greatest impact on cluster enrichment scores and the least variation of clonal enrichment scores within each cluster. Between individual CDRs, L3 contributed the most to enrichment followed by H3. This agrees with previous work which demonstrated that, in synthetic fab libraries, L3 diversity plays a greater role in affinity than the traditional H3 diversity in native repertoires.[19] H1 or H2 showed little correlation with cluster enrichment scores, both of which are known to play a minimal role in antigen specificity. From this analysis, we determined that concatenated CDR sequences would be used for clustering and subsequent candidate selection. We also compared the order of

https://doi.org/10.1021/acscentsci.1c01205
ACS Cent. Sci. 2022, 8, 102−109

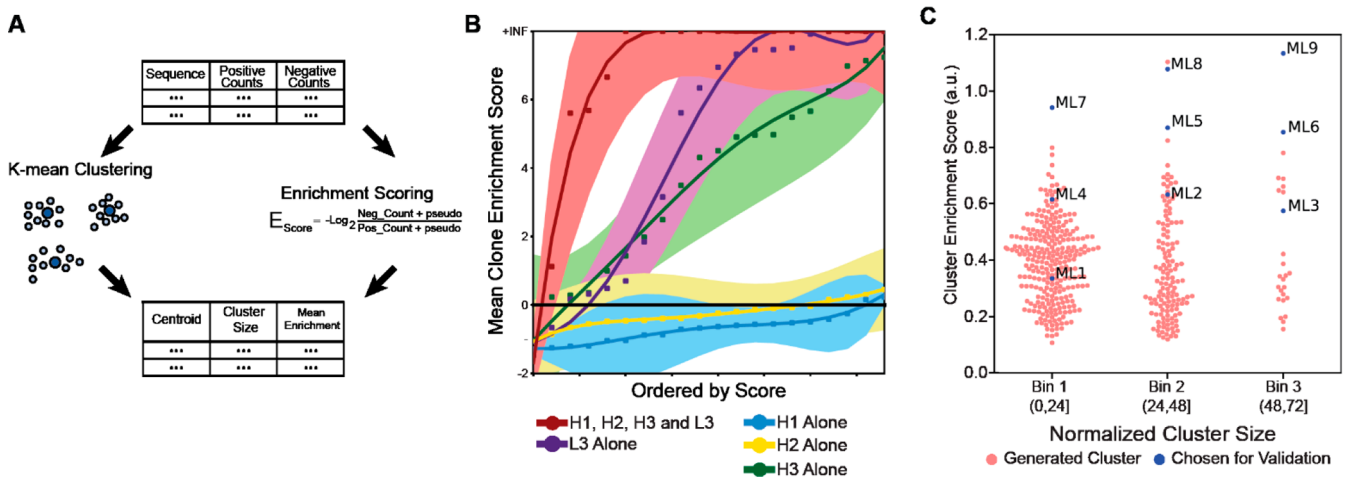

Figure 3. Machine learning candidate selection. (A) Schematic of algorithm. CDR sequences of clones are concatenated and clustered using *k*-means clustering. In parallel, an enrichment score for each clone is calculated using normalized read counts. Centroids from the *k*-means and their cluster size are extracted, and a mean enrichment score for clones within the cluster is calculated. A pseudocount is added to prevent log0 errors. (B) Optimization of *k*-means by comparing which sequence impacts enrichment most. Analysis performed with $k = 20$, ordered along the *x*-axis by score. Error is the standard deviation of the enrichment score. (C) Multiple clustering analyses of round 2 data normalized by *k*-value and plotted against enrichment score. Chosen candidates are highlighted.

concatenation to see if there was an effect on correlation but this analysis did not indicate a significant effect (Figure S3C).

The *k*-means clustering algorithm was then applied on this data set. The cluster sizes were normalized by the *k*-value and compared to the enrichment score of the cluster (Figure 3C).

To choose clones, three candidates from each of the three cluster size bins (ML1 to ML9; ML for machine learning) were selected. By selecting a range of candidates for validation, we sought to understand whether the cluster size or cluster score had the greatest effect on predicting validation success. For medium- and low-scoring clusters, we chose candidates with a high number of reads in all rounds to ensure that the clone enrichment was more statistically significant. In addition, two clones were chosen using a traditional approach (TA1 and TA2; TA for traditional approach) for comparison. To do this, we selected all clones with >100 reads, calculated the fold change in the reads from negative to positive bins, and selected a highly enriched clone—TA1 from round 1 and TA2 from round 2. Sequences, cluster sizes, and scores are provided in Table S1. Only centroids with real clones in the data set were considered.

Candidate Validation. μCellect candidate CDR sequences were cloned into a IgG1 format, expressed, purified, and quantified. Sufficient quantities were achieved for all candidates except ML3 and ML4.

Candidates were first assessed for binding the Fzd7$^+$myc$^+$ or myc$^+$ cells used in the screen. Wild-type (WT) CHO cells were included as a control for nonspecific binding. As a positive control, OMP18R5 in an IgG2 framework was used. OMP18R5 is a Fzd1/2/5/7/8 binder that underwent clinical trials as an oncological therapeutic under the name vantictumab (OncoMed). Three candidates (ML7, ML8, and ML9) showed high affinity to the Fzd7$^+$myc$^+$ target cell line alone (Figure 4A). Other candidates had minimal affinity to the target cell lines. TA1 bound to no cells, and TA2 bound to all cell types. No candidates showed myc affinity. This suggests that the cluster score is a much greater predictor for validation success than cluster size.

A dose−response analysis using ML7, ML8, and ML9 (on-cell in Figure 4B, purified Fzd7 extracellular domain (ECD)/Fc chimera ELISA in Figure 4C) showed that ML9 had an EC50 value comparable to OMP18R5, and other candidates had EC50s less than 10 nM. Candidates' dissociation constants (K_d) against Fzd7, measured via biolayer interferometry, were comparable to OMP19R5 and in the picomolar range (ML7, 448 ± 53 pM; ML8, 4.98 ± 0.28 nM; ML9, 292 ± 66 pM; and OMP18R5, 236 ± 50 pM; Table S2). To test if the candidates could detect endogenous human Fzd7, flow cytometry was performed against a panel of human cell lines with low Fzd7 expression. A HEK293T cell line with CRISPR KO of Fzd7 was included as a negative cell control (Figure 4D).

To assess the specificity of the ML candidates compared to OMP18R5, ELISAs against the ECD of all Frizzled proteins (excluding Fzd3) were performed (Table S3). This analysis revealed that ML7 showed affinity for Frizzled 1/2/7 but minimal affinity to Frizzled 5/8, unlike OMP18R5. This suggests a unique binding behavior of ML7, possibly due to a steric interaction with Frizzled 5/8 or lack of a key residue. To further compare binders, a preliminary epitope binning analysis was performed using a flow cytometric blocking assay (Table S4). A blocking effect was seen for all combinations, but the effect was least when OMP18R5 was the blocking agent. These differences in binding behavior may have clinical relevance given that the trial testing OMP18R5 was halted due to bone-related adverse events, and Fzd8 is a known regulator of bone remodeling.[20] Achieving greater levels of specificity for Fzd7 versus Fzd8 for ML7 is therefore potentially beneficial for clinical applications.

DISCUSSION

Microfluidics has been used to automate traditional biopanning and to perform on-cell selection,[5] control stringency,[21] or eliminate the need for phage elution by on-chip phage lysis,[12] yet few platforms have been widely adopted. Microfluidic phage display would ideally offer a significant reduction in the number of biopanning rounds required or enable discovery of binders for targets with which traditional approaches have had

https://doi.org/10.1021/acscentsci.1c01205
ACS Cent. Sci. 2022, 8, 102−109

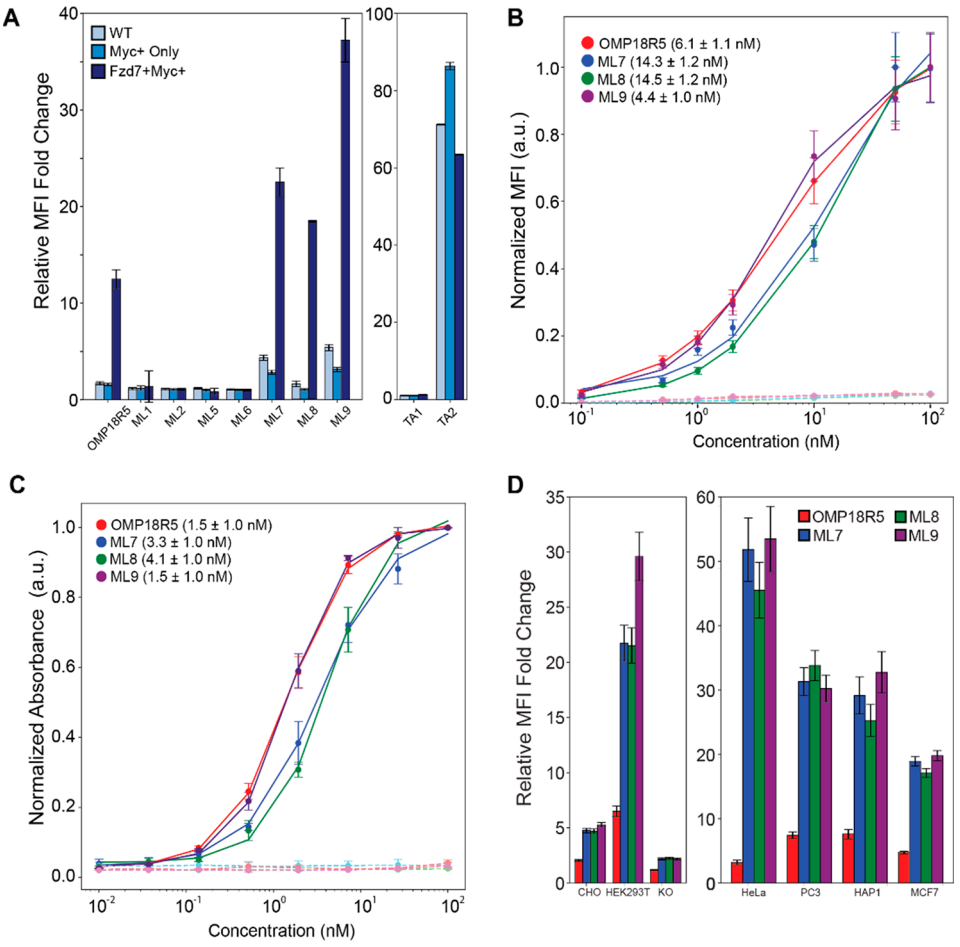

Figure 4. Validation of antibody candidates. (A) Flow cytometry against Fzd7$^+$myc$^+$, myc$^+$, and WT CHO cells. OMP18R5 is a positive control. All candidates at 50 nM. MFI normalized by secondary alone. Error bars indicate a robust coefficient of variation. (B) Flow cytometry of titrated candidates against Fzd7$^+$myc$^+$ cells (solid lines) and WT CHO cells (dotted lines). Four parameter logistic curve fitted with EC50 in parentheses. Normalized by secondary alone and saturation signal. Error bars indicate a robust coefficient of variation. (C) ELISA against purified Frizzled-7/Fc chimera protein (solid lines) shows an affinity to Frizzled-7 extracellular domain. Light dotted lines are against BSA. Four parameter logistics curve fitted with EC50 in parentheses. Normalized by saturation signal. Error bars indicate standard deviation across $N = 3$ technical replicates. (D) Binding to endogenous human Frizzled-7. All candidates at 50 nM. KO is a HEK293T cell line with a CRISPR KO of Fzd1,2,4,5,7. Error bars indicate a robust coefficient of variation.

limited success. μCellect addresses both of these objectives given that only two rounds of selection were required to find high-affinity binders for human Frizzled-7, a challenging target for traditional biopanning.

Fzd7 is therapeutically relevant given its functional role in Wnt signaling and overexpression in breast,[22] glioblastoma,[23] colorectal,[24] and nonsmall cell lung cancers.[25] Fzd7 is also an α-helical G-protein-coupled receptor (GPCR) class transmembrane protein. This class of targets is known to be challenging for phage display.[26−28] This is due to their poor aqueous solubility, high conformational variability, small extracellular regions, and low expression relative to most cell surfactomes.[27] As such, only three successful GPCR-targeting antibodies have been approved by the FDA (anti-CCR4 mogamulizumab, CGRP-inhibitor erenumab, and CCR5 antagonist leronlimab).[29] Fzd7 has been targeted using small molecules,[30] antibodies,[25,31] and siRNA/shRNA knockdown,[24] yet no therapeutics targeting Fzd7 have achieved FDA approval. Therefore, discovering antibodies against such a target with picomolar affinity, unique epitopes, and greater selectivity within the protein family than existing binders is remarkable.

μCellect finds binders to such targets by performing selection in a heterogeneous cell mixture. This is done to recapitulate the complex binding environment where antigens are presented at low concentration and with conformational variability. A selection with mixed cells was first demonstrated in a screen against CCR5 using FACS.[32] μCellect expands on this work by increasing the ratio of cells from 1:4 to 1:20 to increase stringency, thereby achieving binders with 50-fold lower EC50s and using the MICS sorter to drastically increase the throughput and lower the cost of sorting.

Increased throughput enables a larger number of cells to be used (relative to other microfluidic phage display platforms or FACS) thereby sampling the library at a higher rate to eliminate biases due to poor representation.

Although high processing speed is possible with MICS, it is not required. For applications requiring low cell numbers, such as primary cell types, sorting at a low cell concentration (10^4 cells/mL) or isolation of rare cells (1−10 cells/mL of human blood) is possible.[33] Similarly, identification and overexpression of the antigen were performed for this screen but are not required. Target cell types may be captured using identified biomarkers of the cell phenotype, while the specific

https://doi.org/10.1021/acscentsci.1c01205
ACS Cent. Sci. 2022, 8, 102−109

antigen remains unknown or at physiologically relevant surface density, which affects binding dynamics.[34] Although binders to Fzd7 were identified in only two rounds of selection, it is likely that future iterations of μCellect require only one. By negative selection with myc$^+$antigen$^-$ cells in suspension without sorting, the library size could be reduced, and myc binders could be removed, drastically improving the signal-to-noise ratio of the first round of sorting and selection. The MICS platform also requires minimal external setup which makes it amenable for deployment in the biotechnology industry, especially if transitioned to an injection mold fabrication strategy.[35] In addition to improvements made during biopanning, μCellect also offers a valuable technique for choosing candidates for validation. Rather than considering each clone independently from each other, our *k*-means clustering approach identifies trends in the CDR structure across all clones which contribute to enrichment and chooses clones which best represent these trends. An additional strength of this approach is that it is unsupervised—requiring no *a priori* training. Previously, supervised machine learning methods have been used to improve the phage display workflow.[14,15] However, supervision requires preexisting training data which limits their use against novel antigens. μCellect is the first demonstrated use of unsupervised machine learning to choose candidates for validation.

In the proof-of-concept screen, three candidates (ML7, ML8, and ML9) showed high affinity to Fzd7, demonstrating the value of this selection method. Candidates chosen using traditional enrichment analysis (TA1 and TA2) failed to demonstrate antigen-specific binding. ML7, ML8, and ML9 were the highest enriched real clones in their size bin confirming the value of choosing hits based on cluster enrichment scores. Interestingly, ML7 which has a relatively small cluster size was also validated, which suggests that a large cluster size may not be required for validation. Also of note was that the three validated candidates had the same variable heavy chain sequences (H1, H2, and H3). We investigated whether their affinity to Fzd7 was determined by the common heavy chain or the unique CDR L3s. *In silico*, all clones with either the same heavy chain or L3 as the validated hits were identified, and the mean clone enrichment scores for these groups were calculated (Table 1). It was clear that both the common heavy chain and the unique CDR L3s were predictors for enrichment, but the effect was greater for L3. This also agrees with our initial *k*-means analysis, which showed that clustering by L3 resulted in higher cluster enrichment scores than clustering by H3. To confirm this hypothesis *in vitro*, we generated six IgGs with either the same heavy chain or the same L3 as our candidates and tested their affinity by flow cytometry (Figure S2D). Two out of three clones with the same L3 showed specific affinity to Fzd7$^+$ cells, while for the clones with the same heavy chain, two showed no binding, and one showed nonspecific binding to both Fzd7$^+$ and myc$^+$ cells.

Table 1. Mean Enrichment Scores of Clones Appearing in Round 2 Grouped by Commons CDRs

grouping	number of clones	mean enrichment score (R2)
heavy chain	203	1.9541
L3 (ML7)	33	3.7003
L3 (ML8)	32	2.6191
L3 (ML9)	307	2.3824

These results confirm that the unique L3s of ML7, ML8, and ML9 contribute most to Fzd7 binding. These candidates not only demonstrated high affinity to Fzd7, with picomolar dissociation constants, but also generated a stronger signal than first-in-class reagents[36] when detecting low-expression endogenous Fzd7 and had more specificity with the Frizzled protein family. Considering that these candidates were found in two rounds of selection, this underscores the value of μCellect for the rapid discovery of candidates against novel target antigens.

In summary, μCellect is a novel phage display platform which leverages the combined technologies of microfluidics and machine learning to address the challenges associated with conventional phage display. In a two-round on-cell selection against human Frizzled-7 we identified binders with picomolar affinity. This demonstrates the utility and potential for μCellect to gain widespread adoption when pursuing challenging protein targets and/or to reduce antibody development timelines. The low cost and equipment requirements for microfluidics and open-source code enable the deployment of this platform across the biotechnology space.

■ ASSOCIATED CONTENT

Supporting Information

The Supporting Information is available free of charge at https://pubs.acs.org/doi/10.1021/acscentsci.1c01205.

> Detailed methods including mammalian cell line cloning and culture; antibody titrations; phage preparation; cell mixing, phage incubation, and labeling; microfluidic sorting; phage elution and amplification; deep sequencing; data analysis and *k*-means clustering; IgG production; flow cytometry; ELISA; biolayer interferometry; figures including optimization of cell culture and labeling conditions; selection schematic; selection GFP enrichment; distribution of scores in rounds; correlation of CDR concatenation with score; and flow cytometry on candidates with overlapping CDRs; and tables including candidate sequences and scoring; BLI measurements of binding dynamics; pan-Frizzled ELISA; and a blocking assay (PDF)

■ AUTHOR INFORMATION

Corresponding Author

Shana O. Kelley − *Department of Pharmaceutical Sciences, University of Toronto, Toronto, Ontario M5S 3M2, Canada;* orcid.org/0000-0003-3360-5359; Email: shana.kelley@utoronto.ca

Authors

David N. Philpott − *Edward S. Rogers Sr. Department of Electrical & Computer Engineering, University of Toronto, Toronto, Ontario M5S 3G8, Canada*

Surath Gomis − *Edward S. Rogers Sr. Department of Electrical & Computer Engineering, University of Toronto, Toronto, Ontario M5S 3G8, Canada*

Hansen Wang − *Department of Pharmaceutical Sciences, University of Toronto, Toronto, Ontario M5S 3M2, Canada*

Randy Atwal − *Department of Pharmaceutical Sciences, University of Toronto, Toronto, Ontario M5S 3M2, Canada*

Abdellali Kelil − *Donnelly Centre, University of Toronto, Toronto, Ontario M5S 3E1, Canada*

https://doi.org/10.1021/acscentsci.1c01205
ACS Cent. Sci. 2022, 8, 102−109

Tanja Sack − *Department of Pharmaceutical Sciences, University of Toronto, Toronto, Ontario M5S 3M2, Canada*
Brandon Morningstar − *Department of Pharmaceutical Sciences, University of Toronto, Toronto, Ontario M5S 3M2, Canada*
Chris Burnie − *Department of Pharmaceutical Sciences, University of Toronto, Toronto, Ontario M5S 3M2, Canada*
Edward H. Sargent − *Edward S. Rogers Sr. Department of Electrical & Computer Engineering, University of Toronto, Toronto, Ontario M5S 3G8, Canada;* orcid.org/0000-0003-0396-6495
Stephane Angers − *Department of Pharmaceutical Sciences, University of Toronto, Toronto, Ontario M5S 3M2, Canada*
Sachdev Sidhu − *Donnelly Centre, University of Toronto, Toronto, Ontario M5S 3E1, Canada*

Complete contact information is available at: https://pubs.acs.org/10.1021/acscentsci.1c01205

Author Contributions

D.N.P. fabricated devices, optimized sorting conditions, performed sorting and flow cytometry, performed validation experiments, and wrote the manuscript. S.G. performed the *k*-means clustering analysis and assisted with manuscript writing. R.A. aided in experimental design. H.W., T.S., B.M., and C.B. aided in experimental design and prepared phage pools for selection and NGS. A.K. aided in bioinformatic analysis. E.H.S., S.O.K., S.A., and S.S. supervised the study and aided in project guidance. All authors have given approval to the final version of the manuscript.

Funding

This research was supported by the University of Toronto's Medicine by Design initiative, which receives funding from the Canada First Research Excellence Fund (CFREF).

Notes

The authors declare no competing financial interest.

■ ACKNOWLEDGMENTS

D.N.P. would like to thank Peter Aldridge for MICS development, Sichun Lin and Meng Zhang for cell lines, Ben Pinder for sequencing, Maryna Gorelik and Chao Chen for IgG production and purified proteins, Levi Blazer for advice on validation assays, Azza Al Mahrouki and the Centre for Pharmaceutical Oncology, the Toronto Nanofabrication Centre, and the Toronto Recombinant Antibody Centre.

■ ABBREVIATIONS

NGS, next-generation sequencing; MNP, magnetic nanoparticle; MICS, microfluidic cell sorter; CHO, Chinese hamster ovary; MACS, magnetic-activated cell sorting; FACS, fluorescence-activated cell sorting; Fab, fragment-antibody binding; CDR, complementarity determining region; ECD, extracellular domain; Fc, fragment crystallizable; GPCR, G-protein coupled receptor

■ REFERENCES

(1) Ledsgaard, L.; Kilstrup, M.; Karatt-Vellatt, A.; McCafferty, J.; Laustsen, A. H. Basics of Antibody Phage Display Technology. *Toxins* **2018**, *10* (6), 236.
(2) Almagro, J. C.; Pedraza-Escalona, M.; Arrieta, H. I.; Pérez-Tapia, S. M. Phage Display Libraries for Antibody Therapeutic Discovery and Development. *Antibodies* **2019**, *8* (3), 44.
(3) Chen, P.; Nirula, A.; Heller, B.; Gottlieb, R. L.; Boscia, J.; Morris, J.; Huhn, G.; et al. SARS-CoV-2 Neutralizing Antibody LY-CoV555 in Outpatients with Covid-19. *N. Engl. J. Med.* **2021**, *384* (3), 229−237.
(4) Weinreich, D. M.; Sivapalasingam, S.; Norton, T.; Ali, S.; Gao, H.; Bhore, R.; Musser, B. J.; et al. REGN-COV2, a Neutralizing Antibody Cocktail, in Outpatients with Covid-19. *N. Engl. J. Med.* **2021**, *384*, 238−251.
(5) Wang, J.; Liu, Y.; Teesalu, T.; Sugahara, K. N.; Kotamrajua, V. R.; Adams, J. D.; Ferguson, B. S.; et al. Selection of Phage-Displayed Peptides on Live Adherent Cells in Microfluidic Channels. *Proc. Natl. Acad. Sci. U. S. A.* **2011**, *108* (17), 6909−6914.
(6) Rajput, R.; Khanna, M.; Pradhan, H. Phage-Display Technology for the Production of Recombinant Monoclonal Antibodies. *Mater. Methods* **2014**, *4*, 873.
(7) Gallo, E.; Kelil, A.; Bayliss, P. E.; Jeganathan, A.; Egorova, O.; Ploder, L.; Adams, J. J.; et al. *In Situ* Antibody Phage Display Yields Optimal Inhibitors of Integrin A11/B1. *mAbs* **2020**, *12* (1), 1717265.
(8) Lindner, T.; Kolmar, H.; Haberkorn, U.; Mier, W. DNA Libraries for the Construction of Phage Libraries: Statistical and Structural Requirements and Synthetic Methods. *Molecules* **2011**, *16* (2), 1625−1641.
(9) Derda, R.; Tang, S. K. Y.; Li, S. C.; Ng, S.; Matochko, W.; Jafari, M. R. Diversity of Phage-Displayed Libraries of Peptides during Panning and Amplification. *Molecules* **2011**, *16* (2), 1776−1803.
(10) Eisenhardt, S. U.; Schwarz, M.; Bassler, N.; Peter, K. Subtractive Single-Chain Antibody (ScFv) Phage-Display: Tailoring Phage-Display for High Specificity against Function-Specific Conformations of Cell Membrane Molecules. *Nat. Protoc.* **2007**, *2* (12), 3063−3073.
(11) Jones, M. L.; Alfaleh, M. A.; Kumble, S.; Zhang, S.; Osborne, G. W.; Yeh, M.; Arora, N.; et al. Targeting Membrane Proteins for Antibody Discovery Using Phage Display. *Sci. Rep.* **2016**, *6* (1), 26240.
(12) Cung, K.; Slater, R. L.; Cui, Y.; Jones, S. E.; Ahmad, H.; Naik, R. R.; McAlpine, M. C. Rapid, Multiplexed Microfluidic Phage Display. *Lab. Chip* **2012**, *12* (3), 562−565.
(13) Wang, C.-H.; Weng, C.-H.; Che, Y.-J.; Wang, K.; Lee, G.-B. Cancer Cell-Specific Oligopeptides Selected by an Integrated Microfluidic System from a Phage Display Library for Ovarian Cancer Diagnosis. *Theranostics* **2015**, *5* (4), 431−442.
(14) Liu, G.; Zeng, H.; Mueller, J.; Carter, B.; Wang, Z.; Schilz, J.; Horny, G.; et al. Antibody Complementarity Determining Region Design Using High-Capacity Machine Learning. *Bioinformatics* **2020**, *36* (7), 2126−2133.
(15) He, B.; Chen, H.; Li, N.; Huang, J. SAROTUP: A Suite of Tools for Finding Potential Target-Unrelated Peptides from Phage Display Data. *Int. J. Biol. Sci.* **2019**, *15* (7), 1452−1459.
(16) Mair, B.; Aldridge, P. M.; Atwal, R. S.; Philpott, D.; Zhang, M.; Masud, S. N.; Labib, M.; et al. High-Throughput Genome-Wide Phenotypic Screening via Immunomagnetic Cell Sorting. *Nat. Biomed. Eng.* **2019**, *3* (10), 796−805.
(17) Kovaltsuk, A.; Krawczyk, K.; Galson, J. D.; Kelly, D. F.; Deane, C. M.; Trück, J. How B-Cell Receptor Repertoire Sequencing Can Be Enriched with Structural Antibody Data. *Front. Immunol.* **2017**, *8*, 1753.
(18) Colic, M.; Wang, G.; Zimmermann, M.; Mascall, K.; McLaughlin, M.; Bertolet, L.; Lenoir, W. F.; et al. Identifying Chemogenetic Interactions from CRISPR Screens with DrugZ. *Genome Med.* **2019**, *11* (1), 52.
(19) Persson, H.; Ye, W.; Wernimont, A.; Adams, J. J.; Koide, A.; Koide, S.; Lam, R.; Sidhu, S. S. CDR-H3 Diversity Is Not Required for Antigen Recognition by Synthetic Antibodies. *J. Mol. Biol.* **2013**, *425* (4), 803−811.
(20) Albers, J.; Keller, J.; Baranowsky, A.; Beil, F. T.; Catala-Lehnen, P.; Schulze, J.; Amling, M.; Schinke, T. Canonical Wnt Signaling Inhibits Osteoclastogenesis Independent of Osteoprotegerin. *J. Cell Biol.* **2013**, *200* (4), 537−549.

(21) Liu, Y.; Adams, J. D.; Turner, K.; Cochran, F. V.; Gambhir, S. S.; Soh, H. T. Controlling the Selection Stringency of Phage Display Using a Microfluidic Device. *Lab Chip* **2009**, *9* (8), 1033.
(22) Benhaj, K.; Akcali, K. C.; Ozturk, M. Redundant Expression of Canonical Wnt Ligands in Human Breast Cancer Cell Lines. *Oncol. Rep.* **2006**, *15* (3), 701−707.
(23) Schiffgens, S.; Wilkens, L.; Brandes, A. A.; Meier, T.; Franceschi, E.; Ermani, M.; Hartmann, C.; et al. Sex-Specific Clinicopathological Significance of Novel (Frizzled-7) and Established (MGMT, IDH1) Biomarkers in Glioblastoma. *Oncotarget* **2016**, *7* (34), 55169−55180.
(24) Ueno, K.; Hazama, S.; Mitomori, S.; Nishioka, M.; Suehiro, Y.; Hirata, H.; Oka, M.; et al. Down-Regulation of Frizzled-7 Expression Decreases Survival, Invasion and Metastatic Capabilities of Colon Cancer Cells. *Br. J. Cancer* **2009**, *101* (8), 1374−1381.
(25) Gurney, A.; Axelrod, F.; Bond, C. J.; Cain, J.; Chartier, C.; Donigan, L.; Fischer, M.; et al. Wnt Pathway Inhibition via the Targeting of Frizzled Receptors Results in Decreased Growth and Tumorigenicity of Human Tumors. *Proc. Natl. Acad. Sci. U. S. A.* **2012**, *109* (29), 11717−11722.
(26) Huang, R.; Kiss, M. M.; Batonick, M.; Weiner, M. P.; Kay, B. K. Generating Recombinant Antibodies to Membrane Proteins through Phage Display. *Antibodies* **2016**, *5* (2), 11.
(27) Ayoub, M. A.; Crépieux, P.; Koglin, M.; Parmentier, M.; Pin, J.-P.; Poupon, A.; Reiter, E.; et al. Antibodies Targeting G Protein-Coupled Receptors: Recent Advances and Therapeutic Challenges. *mAbs* **2017**, *9* (5), 735−741.
(28) Vithayathil, R.; Hooy, R. M.; Cocco, M. J.; Weiss, G. A. The Scope of Phage Display for Membrane Proteins. *J. Mol. Biol.* **2011**, *414* (4), 499−510.
(29) Hutchings, C. J. A Review of Antibody-Based Therapeutics Targeting G Protein-Coupled Receptors: An Update. *Expert Opin. Biol. Ther.* **2020**, *20* (8), 925−935.
(30) Zhang, W.; Lu, W.; Ananthan, S.; Suto, M. J.; Li, Y. Discovery of Novel Frizzled-7 Inhibitors by Targeting the Receptor's Transmembrane Domain. *Oncotarget* **2017**, *8* (53), 91459−91470.
(31) Pavlovic, Z.; Adams, J. J.; Blazer, L. L.; Gakhal, A. K.; Jarvik, N.; Steinhart, Z.; Robitaille, M.; et al. A Synthetic Anti-Frizzled Antibody Engineered for Broadened Specificity Exhibits Enhanced Anti-Tumor Properties. *mAbs* **2018**, *10* (8), 1157−1167.
(32) Shimoni, M.; Herschhorn, A.; Britan-Rosich, Y.; Kotler, M.; Benhar, I.; Hizi, A. The Isolation of Novel Phage Display-Derived Human Recombinant Antibodies Against CCR5, the Major Co-Receptor of HIV. *Viral Immunol.* **2013**, *26* (4), 277−290.
(33) Aldridge, P. M.; Mukhopadhyay, M.; Ahmed, S. U.; Zhou, W.; Christinck, E.; Makonnen, R.; Sargent, E. H.; Kelley, S. O. Prismatic Deflection of Live Tumor Cells and Cell Clusters. *ACS Nano* **2018**, *12* (12), 12692−12700.
(34) Bastings, M. M. C.; Helms, B. A.; van Baal, I.; Hackeng, T. M.; Merkx, M.; Meijer, E. W. From Phage Display to Dendrimer Display: Insights into Multivalent Binding. *J. Am. Chem. Soc.* **2011**, *133* (17), 6636−6641.
(35) Lee, U. N.; Su, X.; Guckenberger, D. J.; Dostie, A. M.; Zhang, T.; Berthier, E.; Theberge, A. B. Fundamentals of Rapid Injection Molding for Microfluidic Cell-Based Assays. *Lab Chip* **2018**, *18* (3), 496−504.
(36) Smith, D. C.; Rosen, L. S.; Chugh, R.; Goldman, J. W.; Xu, L.; Kapoun, A.; Brachmann, R. K.; et al. First-in-Human Evaluation of the Human Monoclonal Antibody Vantictumab (OMP-18R5; Anti-Frizzled) Targeting the WNT Pathway in a Phase I Study for Patients with Advanced Solid Tumors. *J. Clin. Oncol.* **2013**, *31* (15), 2540−2540.

https://doi.org/10.1021/acscentsci.1c01205
ACS Cent. Sci. 2022, 8, 102−109